Supporting Information

Alkali metal-selenium battery with wide temperature range and low self-discharge

Xiaosen Zhao[a], Lichang Yin[b], Zhenzhen Yang[a,b], Gang Chen[a], Huijuan Yue[c], Dong Zhang[a,*], Zhenhua Sun[b,*], and Feng Li[b,*]

[a] *Key Laboratory of Physics and Technology for Advanced Batteries (Ministry of Education), College of Physics, Jilin University, Changchun 130012, China.*

[b] *Institute of Metal Research, Chinese Academy of Sciences, Shenyang 110016, China.*

[c] *State Key Laboratory of Inorganic Synthesis and Preparative Chemistry, College of Chemistry, Jilin University, Changchun 130012, China.*

**E-mail: dongzhang@jlu.edu.cn (D. Zhang); zhsun@imr.ac.cn (Z. H. Sun); fli@imr.ac.cn (F. Li)*

Figures

Tables

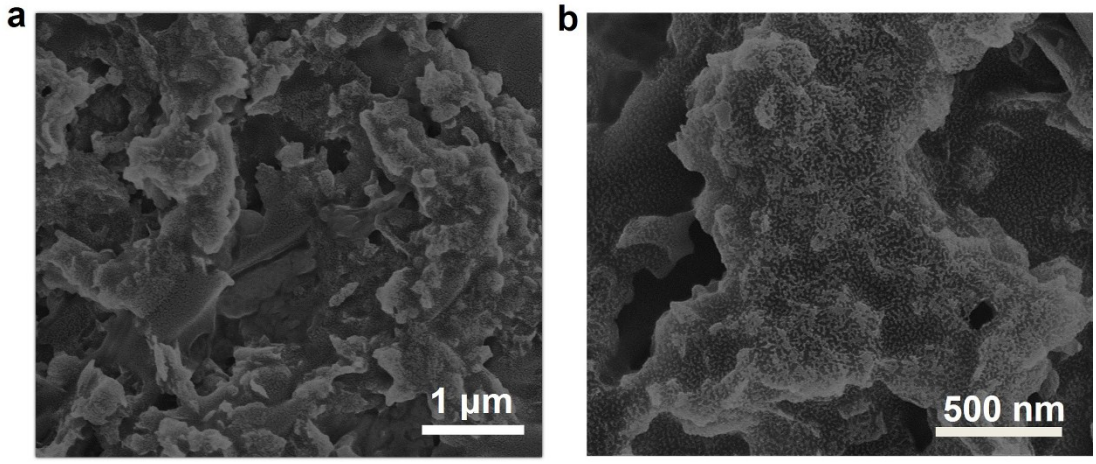

Fig. S1 SEM images of the as-prepared PEDOT in different magnifications.

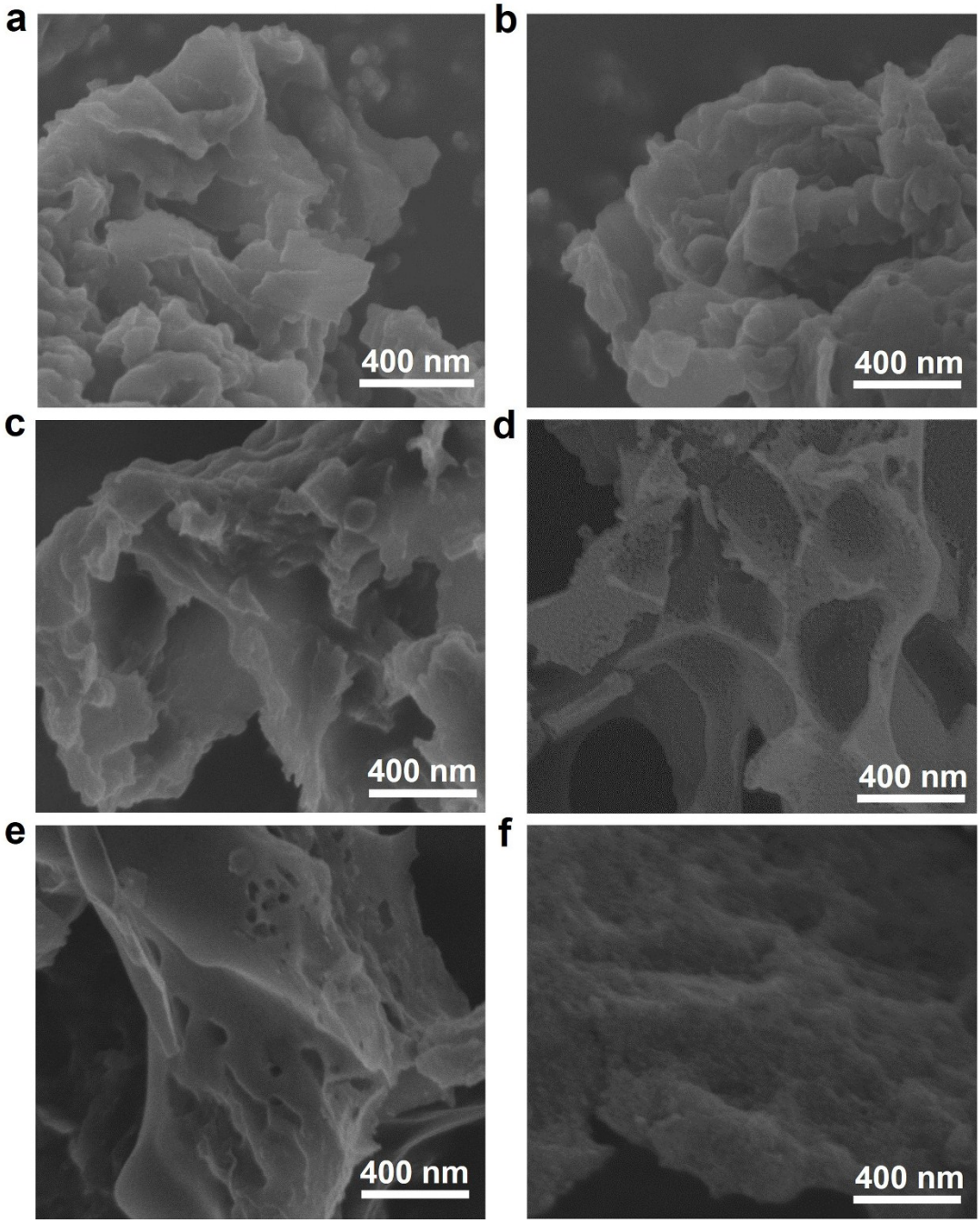

Fig. S2 Morphology characterization of SO-HPC$_x$. SEM images of SO-HPC samples obtained at various mass ratios of KOH to PEDOT: (a) SO-HPC$_0$; (b) SO-HPC$_1$; (c) SO-HPC$_2$; (d) SO-HPC$_3$; (e) SO-HPC$_4$; (f) SO-HPC$_5$.

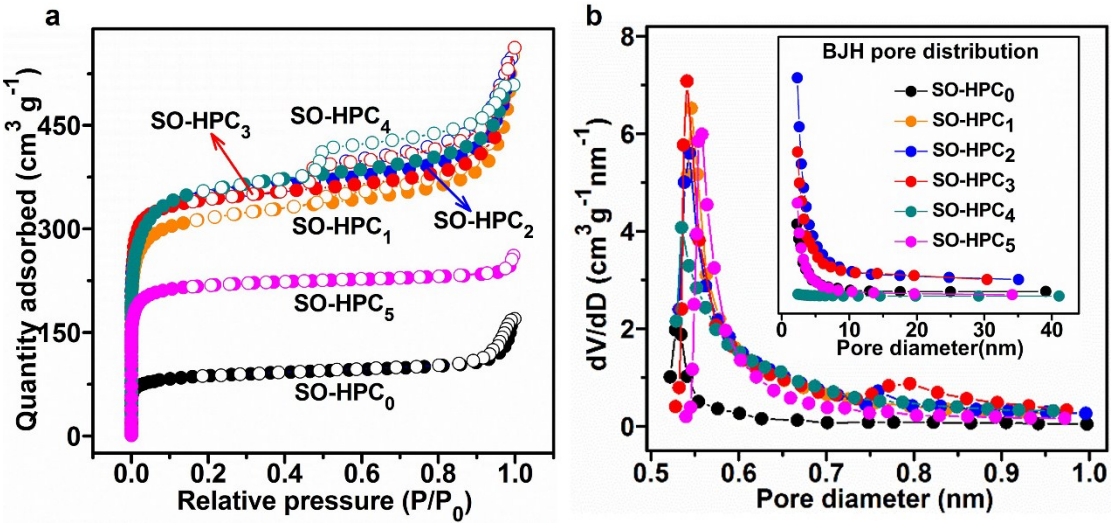

Fig. S3 (a) Nitrogen adsorption/desorption isotherms and (b) micropore distribution of SO-HPC$_x$ (x=0, 1, 2, 3, 4, 5). Insert of Fig. S3b is the mesopore distribution of SO-HPC$_x$ (x=0, 1, 2, 3, 4, 5).

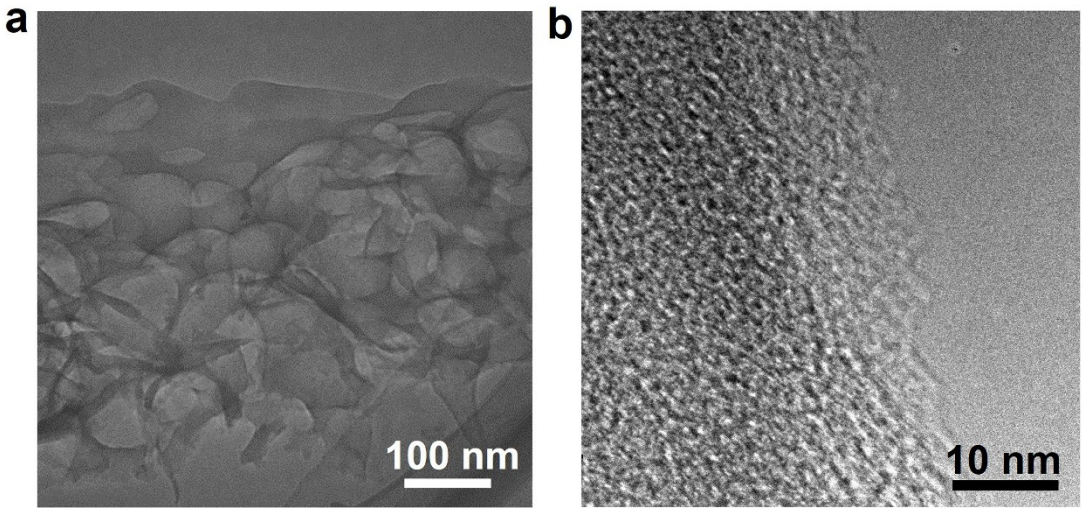

Fig. S4 (a) TEM and (b) HRTEM images of SO-HPC_3.

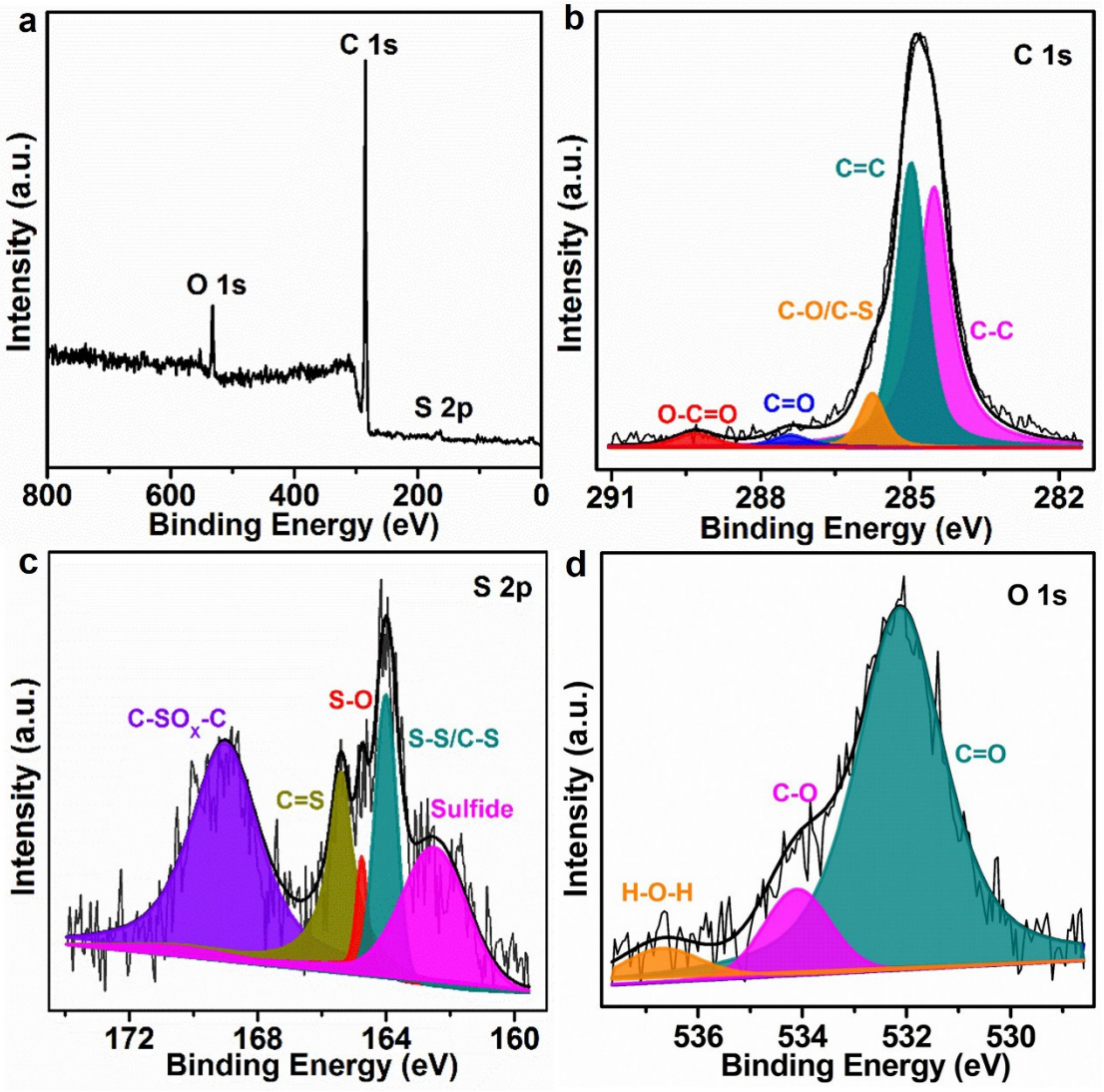

Fig. S5 (a) Overall XPS spectrum of SO-HPC$_3$. High-resolution (b) C1s, (c) S 2p and (d) O1s XPS spectrum of SO-HPC$_3$.

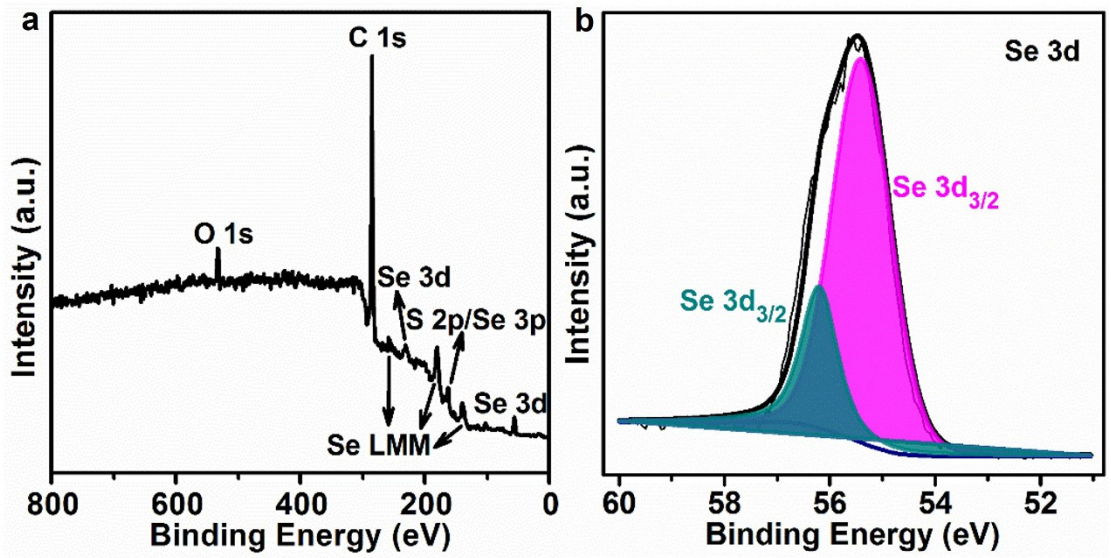

Fig. S6 (a) Overall XPS spectrum of Se_{50}/SO-HPC_3. (b) High-resolution Se 3d XPS spectrum of pristine Se.

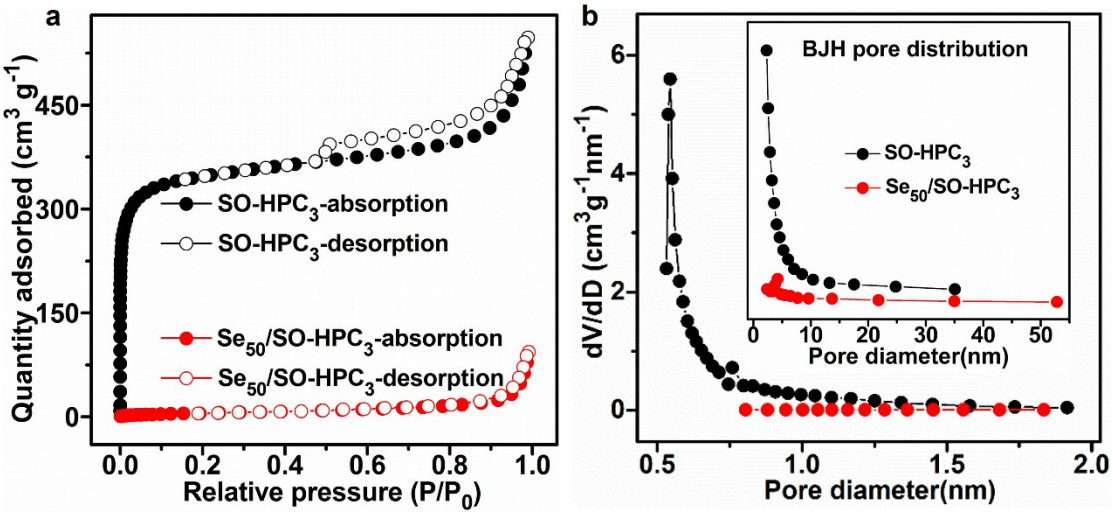

Fig. S7 (a) Nitrogen (N_2) adsorption-desorption isotherms and (b) micropore and mesopore (insert of Fig. S7b) distribution profiles of SO-HPC_3 and Se_{50}/SO-HPC_3.

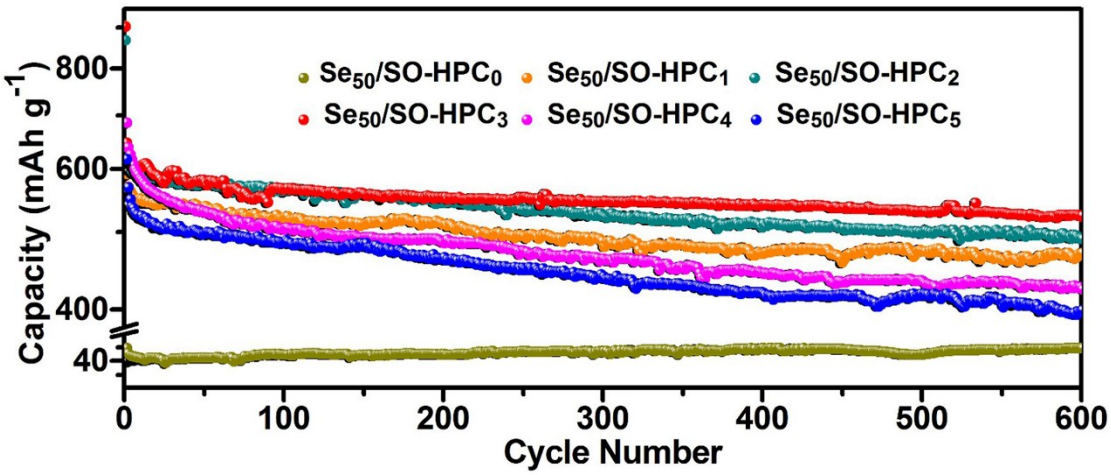

Fig. S8 Cycling performances of Se/SO-HPC$_x$ (x=0, 1, 2, 3, 4, 5) cathodes at a current density of 0.5 C with 50 wt.% Se-loading amount in the cut off voltage range of 1.0-3.0 V for Li-Se battery. The electrochemical performance of Se_{50}/SO-HPC$_x$ (x=0, 1, 2, 3, 4, 5) for Li-Se batteries were tested to evaluate the effect of KOH. The SO-HPC$_3$ derived from a suitable etch ratio with high specific surface area and high micropore volume not only could buffer the electrode volume change, but also prevent the side reaction between Se anions and electrolytes. Besides, the high mechanical strength (fragile framework) caused by moderate activation etching with appropriate amount of KOH and the high conductivities lead to satisfactory electrochemical properties of Se_{50}/SO-HPC$_3$.

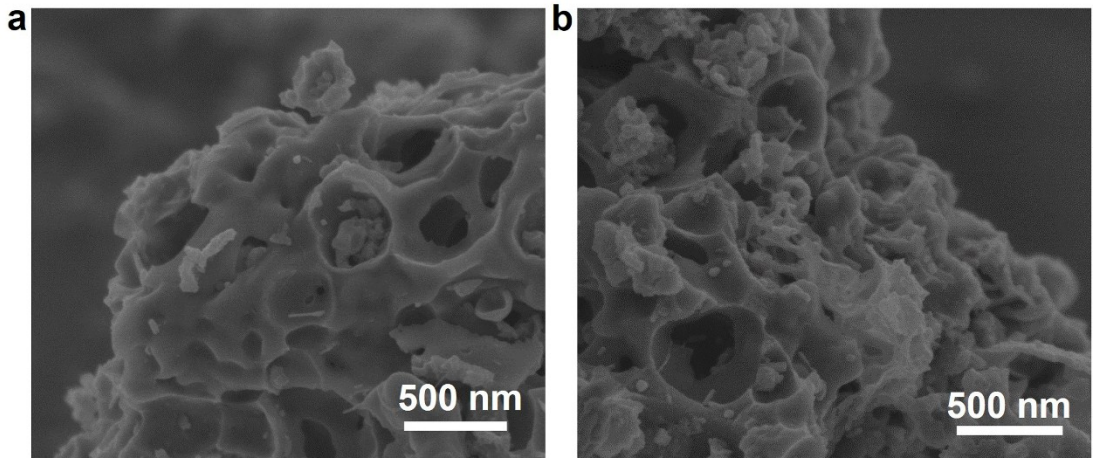

Fig. S9 (a) SEM images of Se_{60}/SO-HPC_3 and (b) Se_{70}/SO-HPC_3. The SEM image of Se_{60}/SO-HPC_3 (Fig. S9a) shows a similar morphology to that of Se_{50}/SO-HPC_3, while a large amount of aggregated Se particles appear on the surface of Se_{70}/SO-HPC_3 (Fig. S9b).

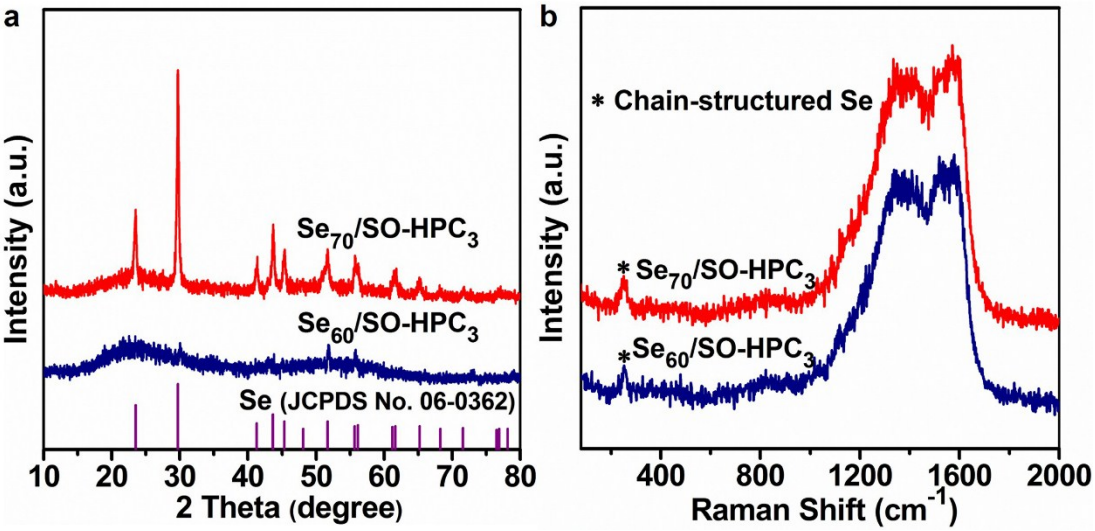

Fig. S10 (a) XRD patterns and (b) Raman spectra of Se_{60}/SO-HPC_3 and Se_{70}/SO-HPC_3. The reemerging characteristic diffraction peaks of Se in XRD (Fig. S10a) and Raman (Fig. S10b) confirm the presence of excessive Se in a crystalline state on the carbon matrix surface.

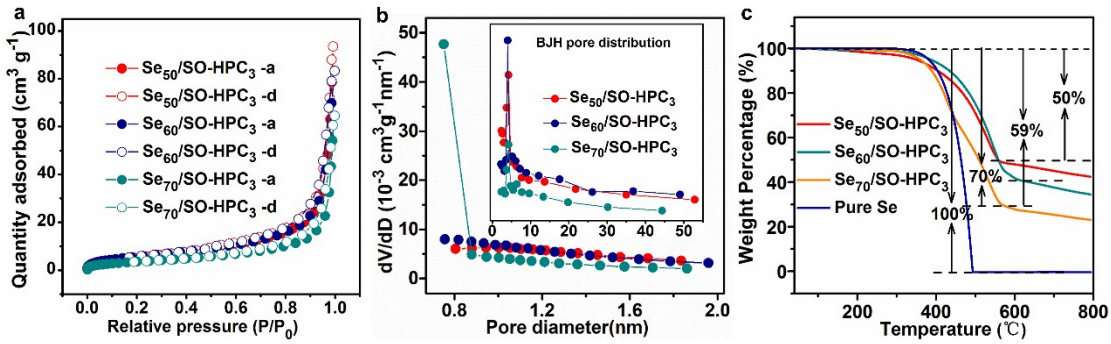

Fig. S11 (a) Nitrogen adsorption-desorption isotherms, (b) micropore distribution, mesopore (insert of Fig. S11b) distribution and TGA curves of Se_{50}/SO-HPC_3, Se_{60}/SO-HPC_3 and Se_{70}/SO-HPC_3. The TGA test results (Fig. S11c) confirm the Se loading amount and the different evaporation temperatures resulting from Se storage in different pore framework.

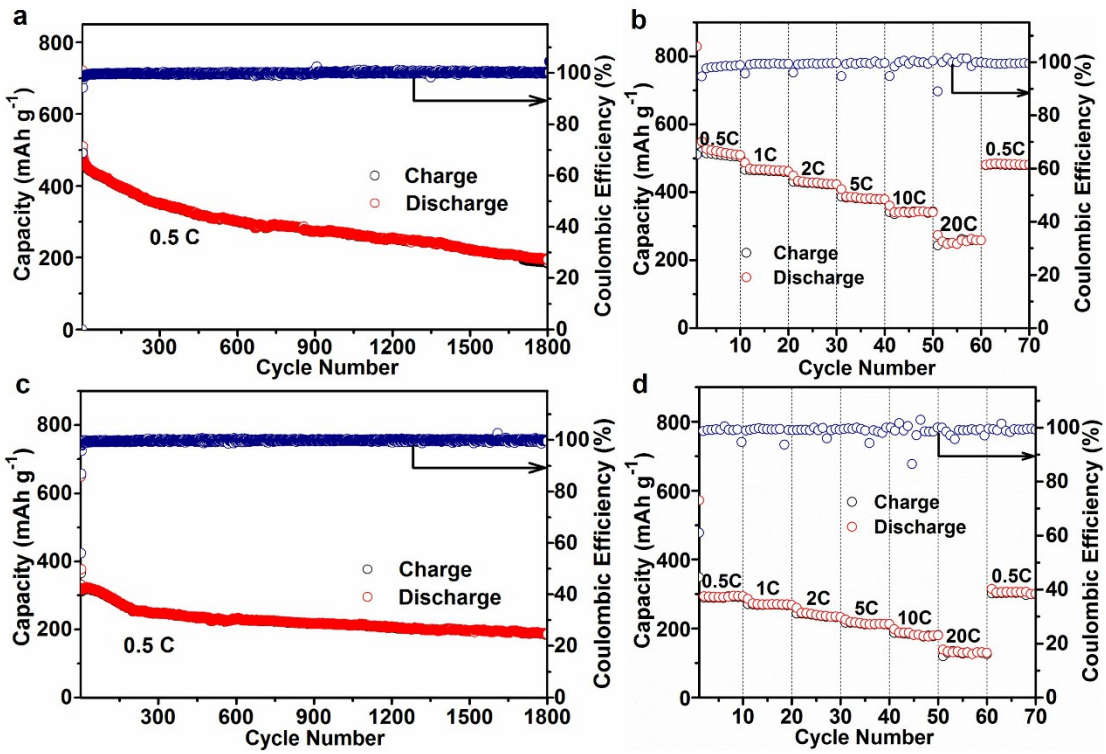

Fig. S12 Eletrochemical performances of Se_{60}/SO-HPC_3 and Se_{70}/SO-HPC_3 cathode. (a) Cycling stability of Se_{60}/SO-HPC_3 at a current density of 0.5 C in the cut off voltage range of 1.0-3.0 V and (b) rate capability of Se_{60}/SO-HPC_3 for Li-Se batteries. (c) Cycling stability of Se_{70}/SO-HPC_3 at a current density of 0.5 C in the cut off voltage range of 1.0-3.0 V and (d) rate capability of Se_{70}/SO-HPC_3 for Li-Se batteries.

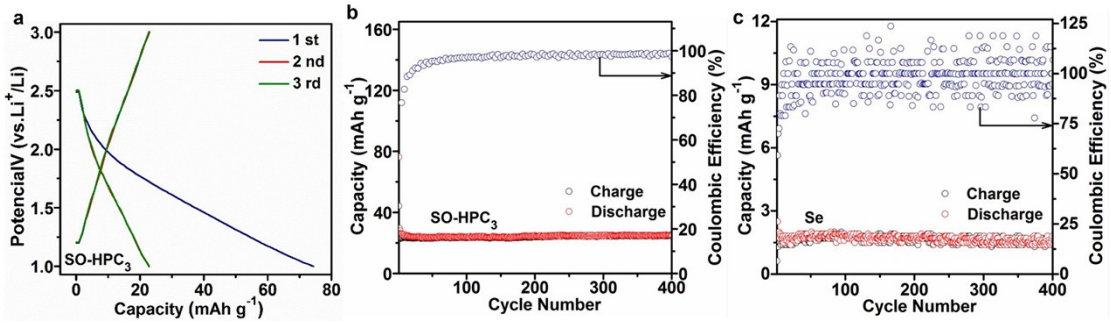

Fig. S13 Eletrochemical performances of SO-HPC_3 and Se cathode. (a) Galvanostatic discharge-charge curves of SO-HPC_3 at 0.5 C. Cycling performance of (b) pristine SO-HPC_3 and (c) Se at a current density of 0.5 C in the cut off voltage range of 1.0-3.0 V for Li-Se battery.

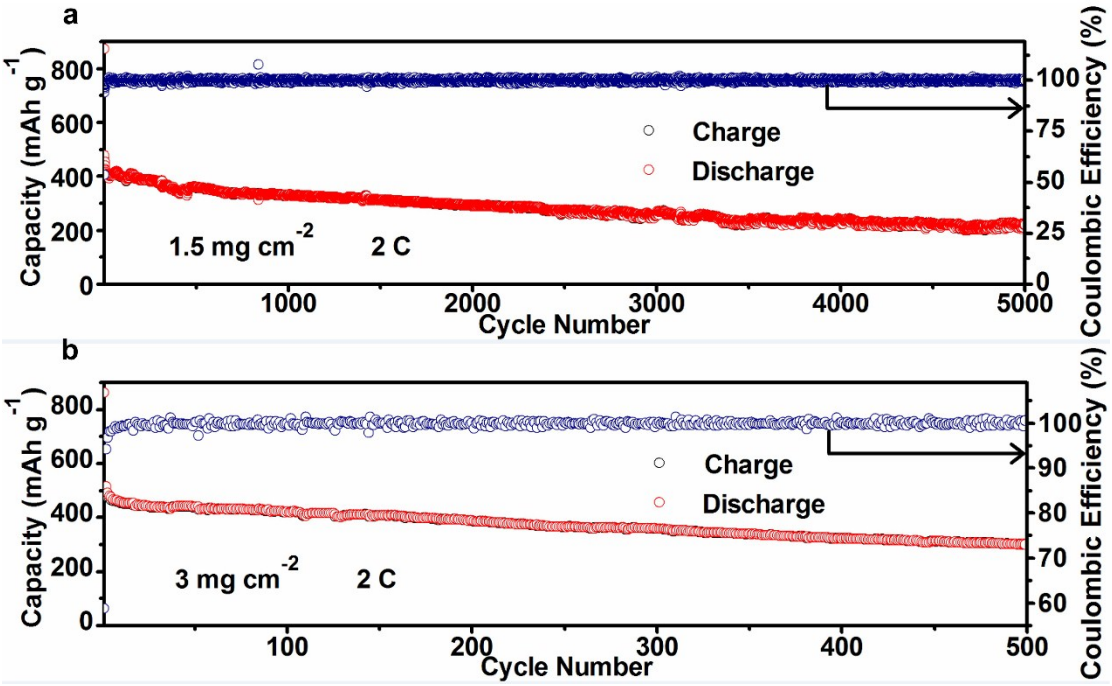

Fig. S14 Eletrochemical performances of Se_{50}/SO-HPC_3 cathode with different area coposite loading. (a) Cycle stability of Se_{50}/SO-HPC_3 in Li-Se battery at 2 C with an area loading of 1.5 mg cm^{-2} for 5000 cycles. (b) Cycle stability of Se_{50}/SO-HPC_3 in Li-Se battery at 2 C with an area composite loading of 3 mg cm^{-2}.

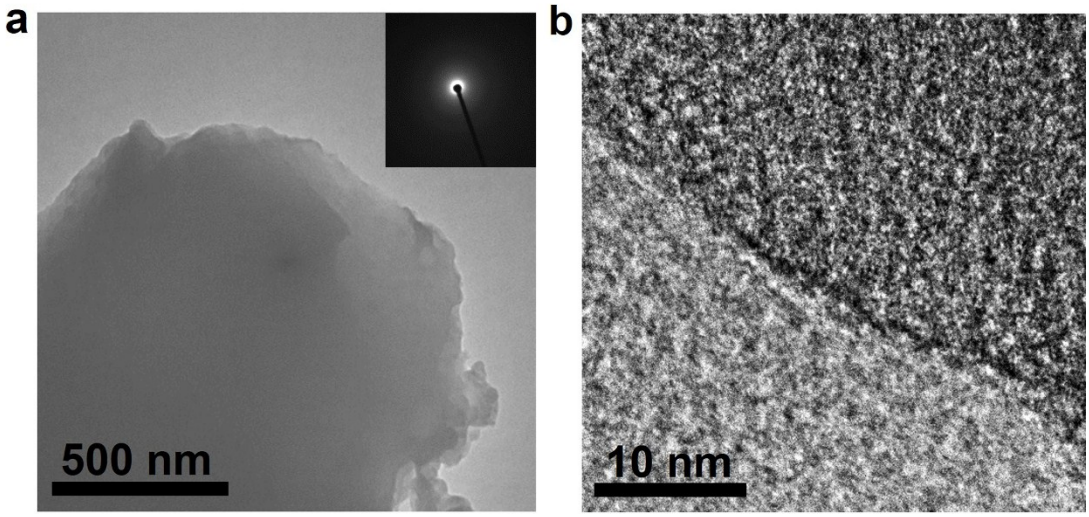

Fig. S15 (a) TEM and (b) HRTEM imgaes of Se_{50}/SO-HPC_3 after 1700 cycles at 0.5 C. The insert of Fig. S15a is its SAED pattern.

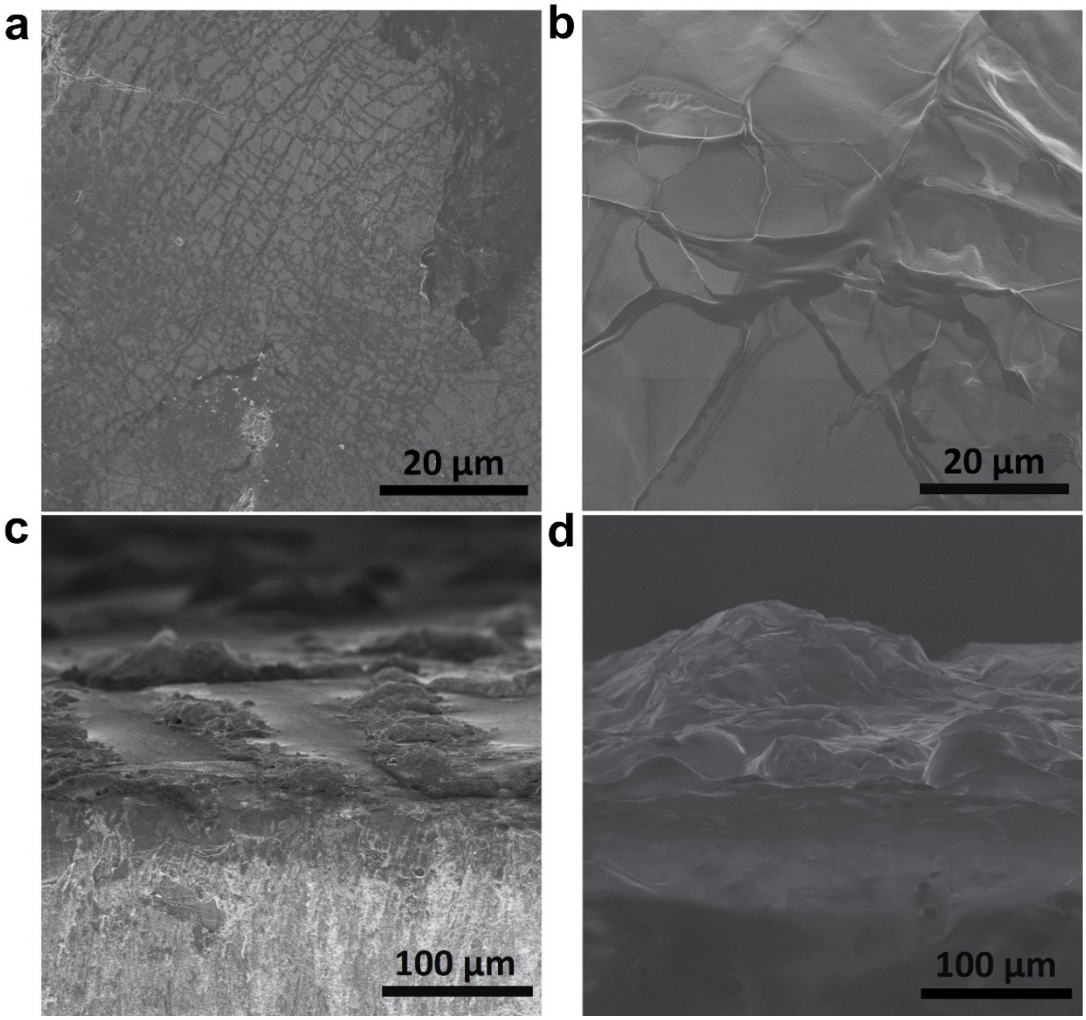

Fig. S16 SEM of the front and cross section of the lithium sheet from the cells after 1700 cycles at 0.5 C with Se_{50}/SO-HPC_3 (a and c) and Se (b and d) cathode.

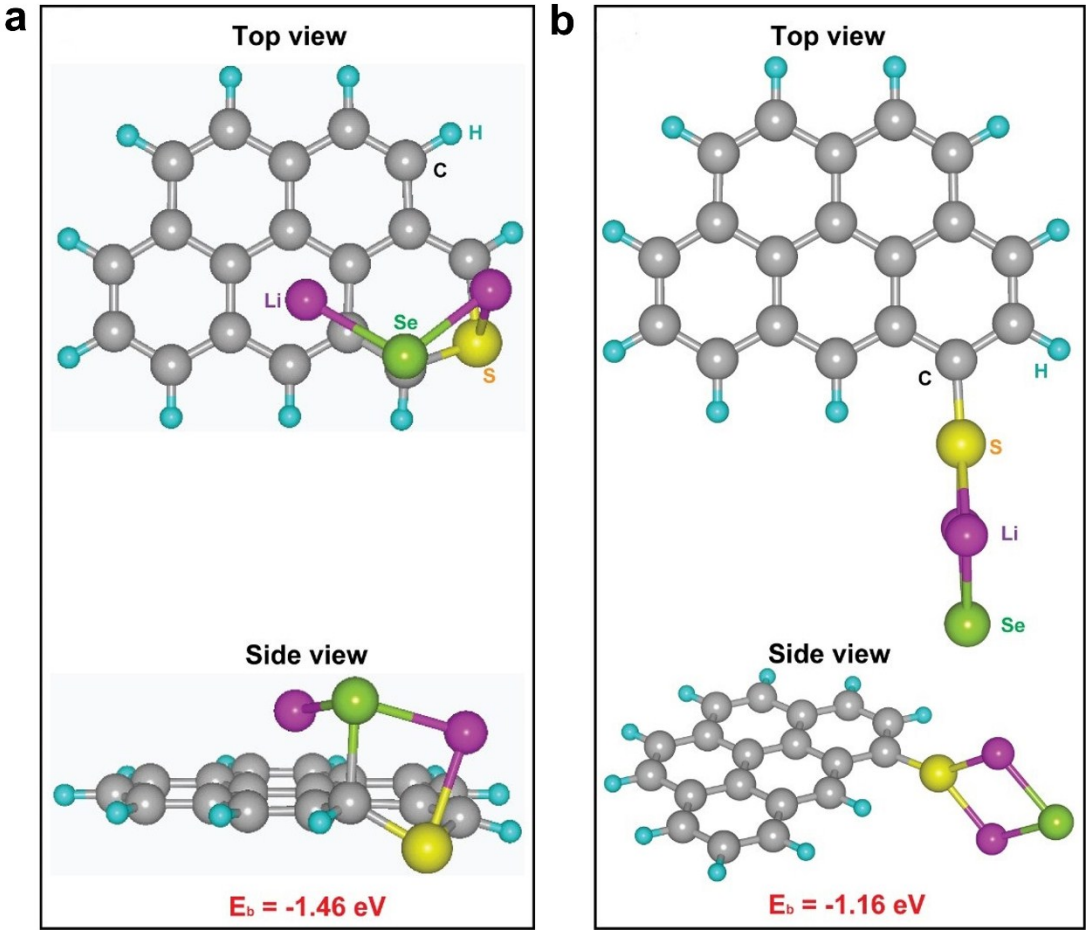

Fig. S17 The interaction of SO-HPC_3 composite with $LiSe_2$. Schematic adsorption configuration of Li_2Se on carbon only with S-doping. The calculated binding energies (in eV) are also presented.

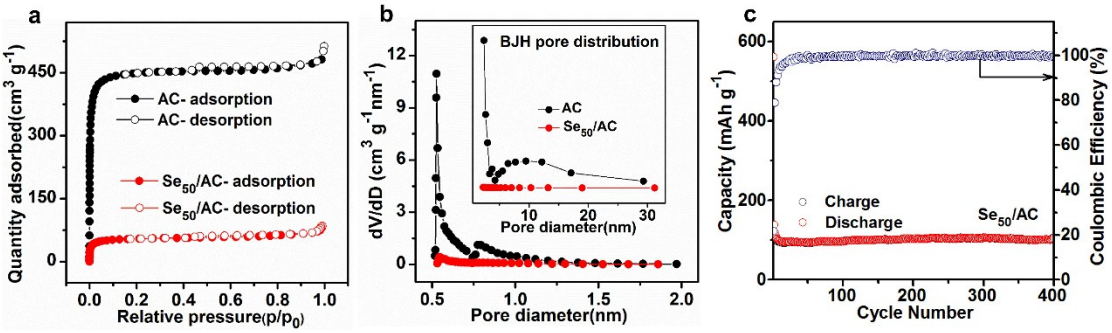

Fig. S18 (a) Nitrogen adsorption-desorption isotherms, (b) micropore distribution and mesopore (insert of Fig. S18b) size distribution of AC and Se_{50}/AC. (c) Electrochemical performance of Se_{50}/AC in Li-Se batteries at 0.5 C in the cut off voltage range of 1.0-3.0 V.

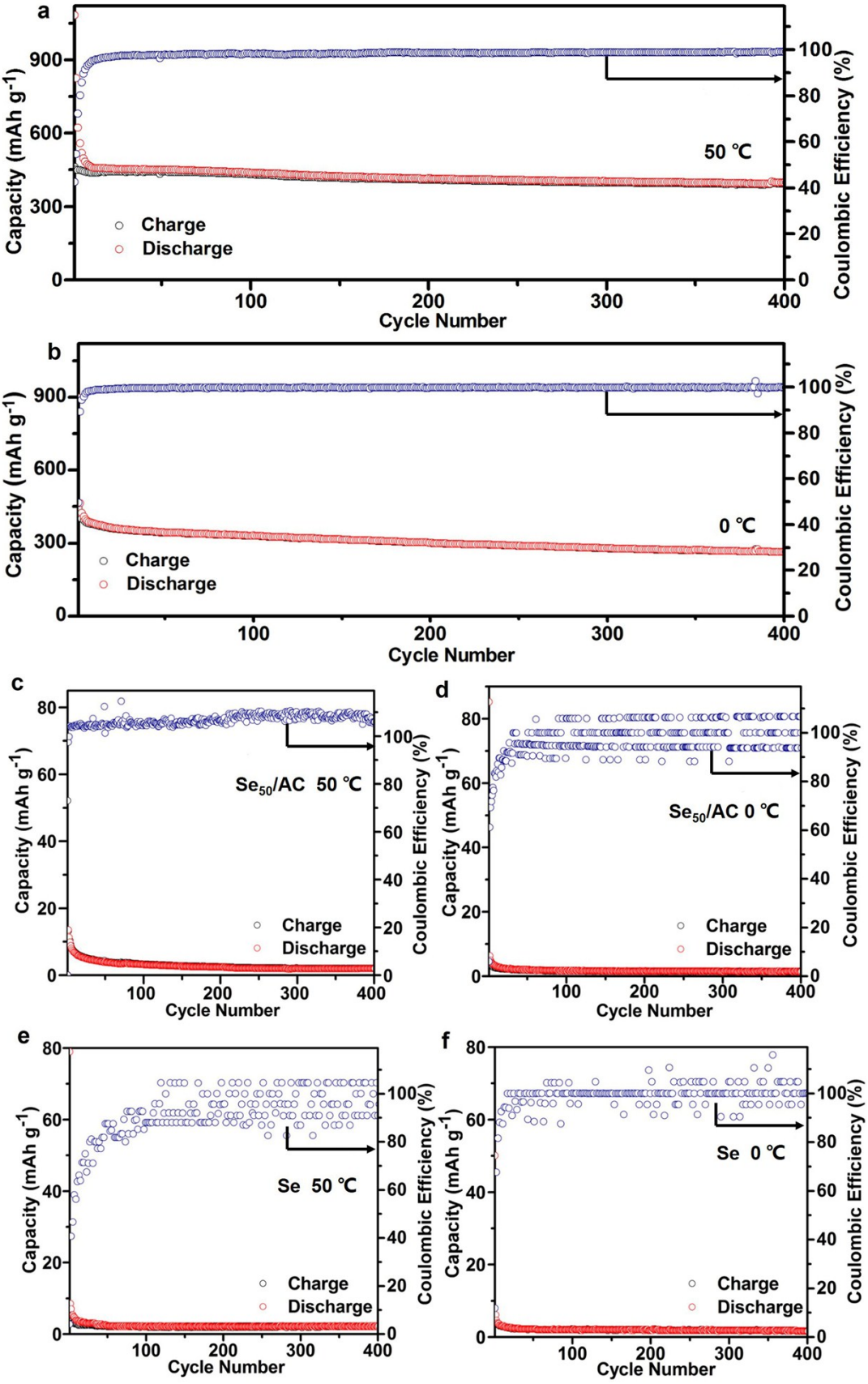

Fig. S19 Cycling performances of Se_{50}/SO-HPC_3 (a and b), Se_{50}/AC (c and d) and Se (e and f) cathodes at 50 °C and 0 °C, respectively, with 0.5 C for Li-Se batteries.

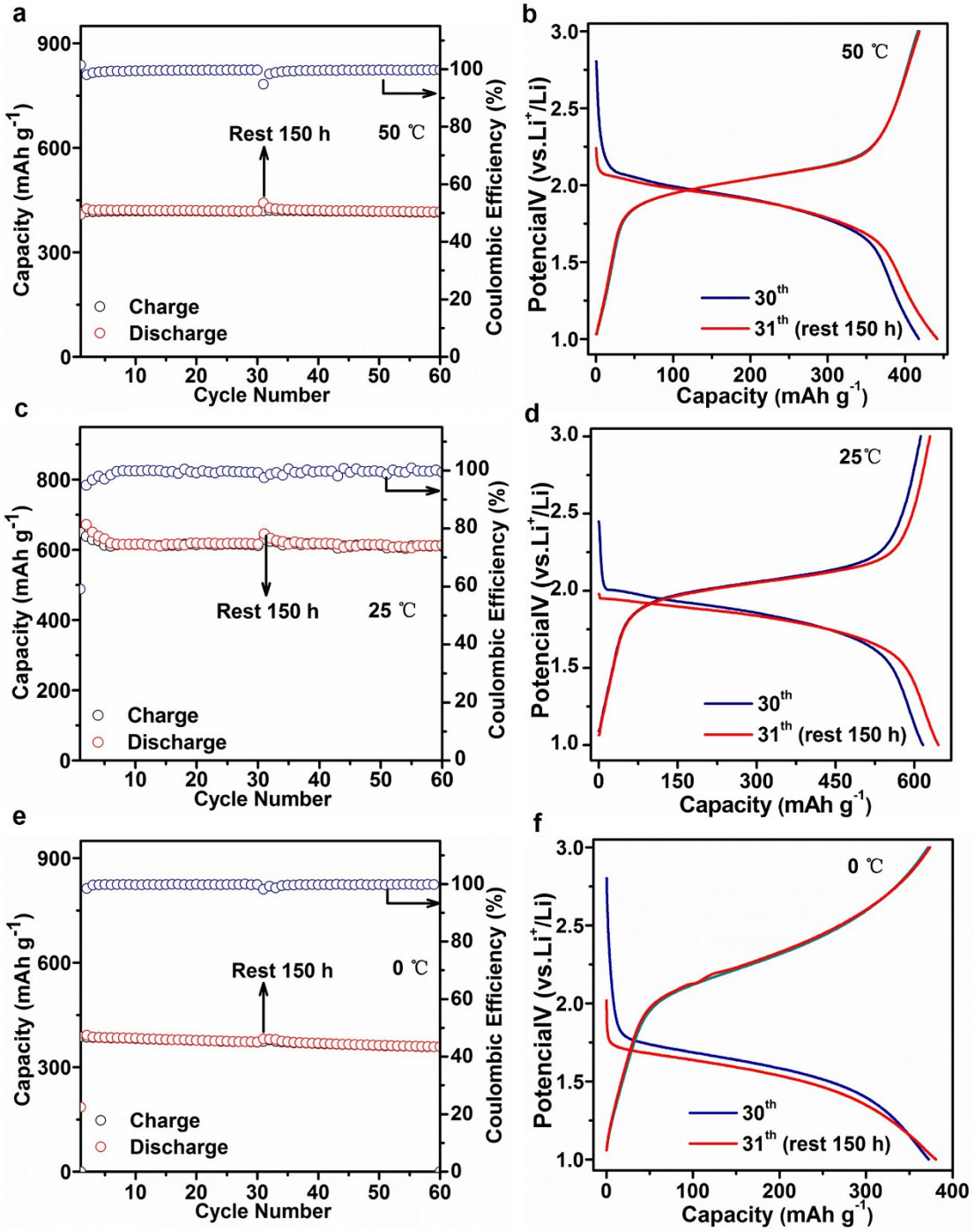

Fig. S20 Self-discharge behavior of Li-Se batteries with Se_{50}/SO-HPC_3 cathodes after an uninterrupted 30 cycles at 0.5 C for Li-Se batteries. Cyclic performance and galvanostatic charge/discharge curves of the cathode materials before and after a rest period of 150 h at 50 °C (a and b), 25 °C (c and d) and 0 °C (e and f) for Li-Se batteries.

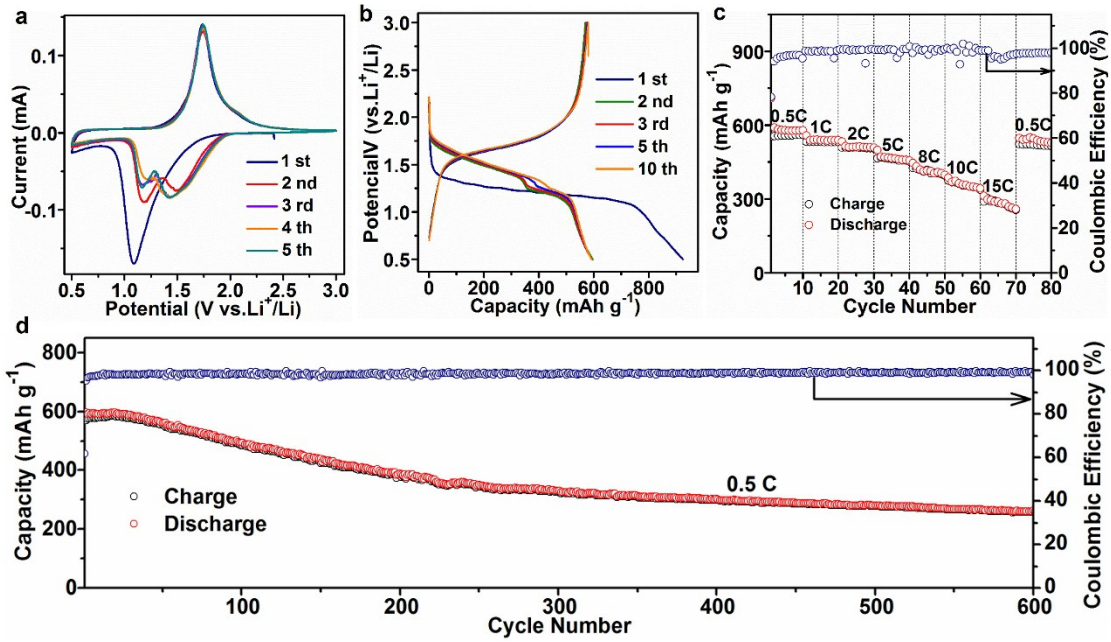

Fig. S21 Eletrochemical performances of Se_{50}/SO-HPC_3 cathode in Na-Se batteries. (a) CV curves of Se_{50}/SO-HPC_3 at a scan rate of 0.1 mV s^{-1} in the cut off voltage range of 0.5-3.0 V vs. Na/Na^+. (b) Galvanostatic discharge-charge curves of Se_{50}/SO-HPC_3 for different cycles at 0.5 C for Na-Se batteries. (c) Rate capability and (d) cycling performance of Se_{50}/SO-HPC_3 at 0.5 C for Na-Se batteries.

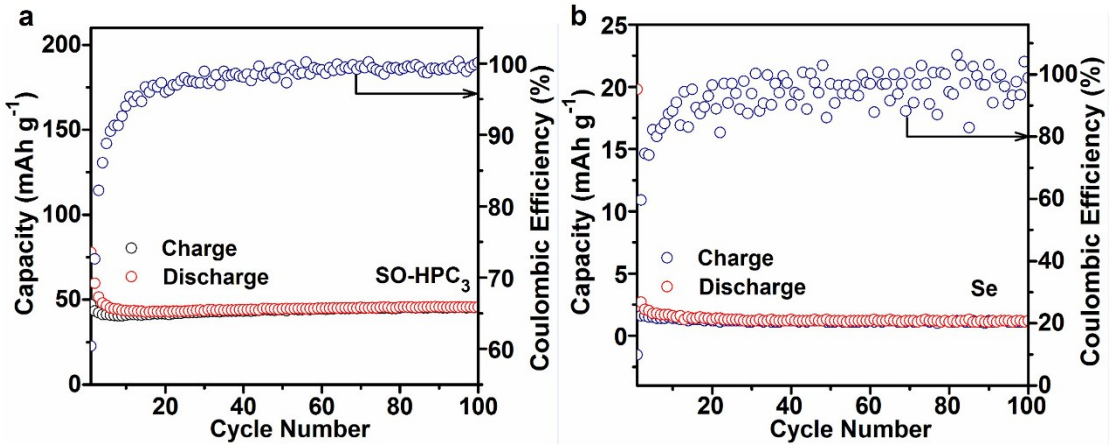

Fig. S22 Cycling performance of (a) pristine SO-HPC_3 and (b) Se for sodium battery at 0.5 C in the cut off voltage range of 0.5-3.0 V.

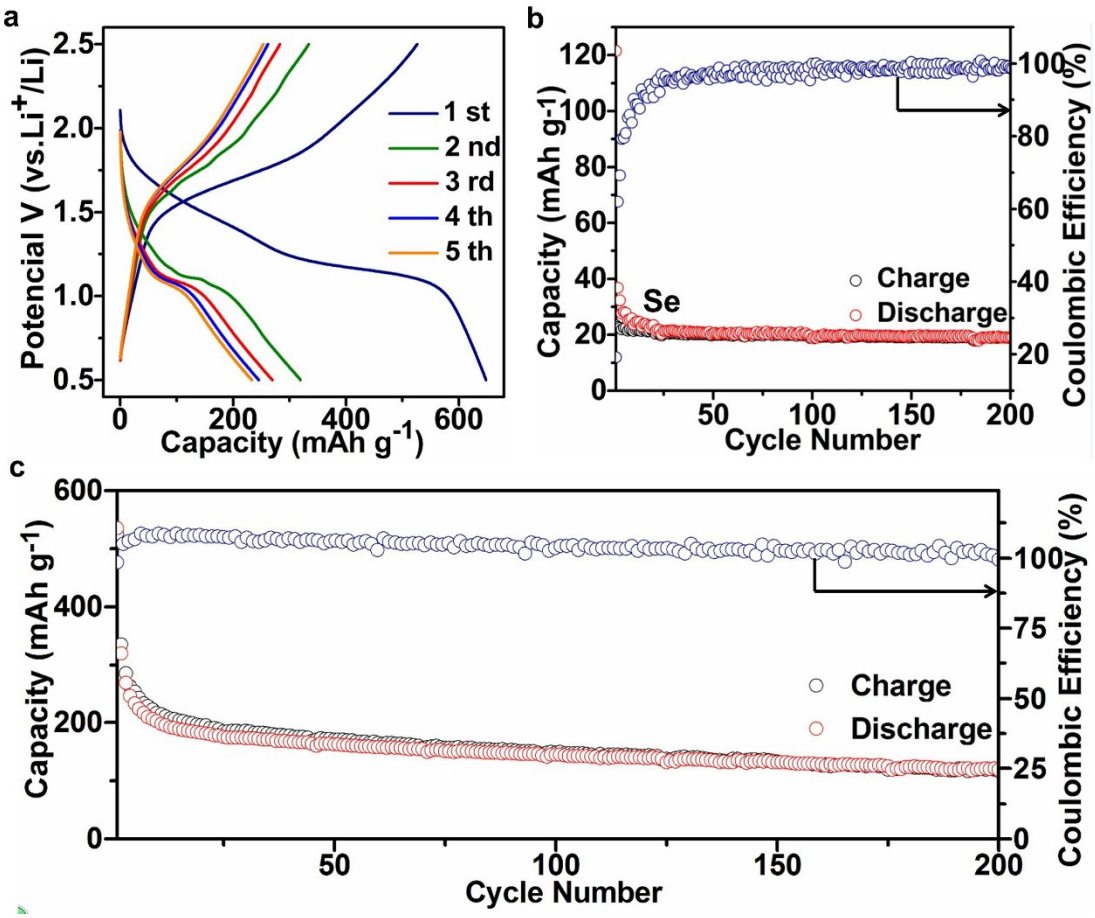

Fig. S23 Eletrochemical performances of Se_{50}/SO-HPC_3 and Se cathode in K-Se batteries. (a) Galvanostatic discharge-charge curves of Se_{50}/SO-HPC_3 for different cycles at 0.5 C in the cut off voltage range of 0.5-2.5 V vs. K/K^+ for K-Se batteries. Cycling performance of (b) Se and (c) Se_{50}/SO-HPC_3 at 0.5 C for potassium batterie

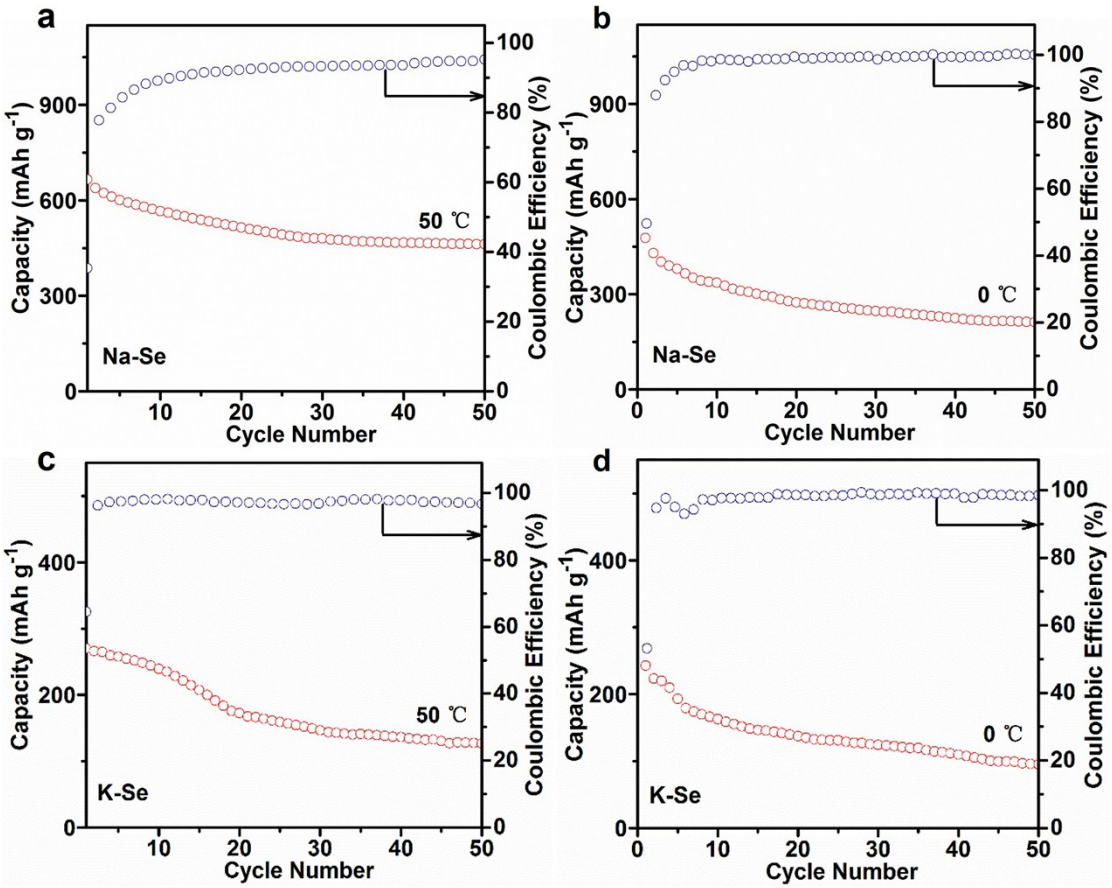

Fig. S24 The cycle performances of Se_{50}/SO-HPC_3 cathodes in Na-Se (a and b) and K-Se (c and d) cells at 50 °C and 0 °C at a current density of 0.5 C.

Table S1 Electrode materials test temperature statistics table.

System	Samples	0 °C	25 °C	50 °C
LIB	$Se_{50}/SO\text{-}HPC_x$ (x=0, 1, 2, 4, 5)	√	/	/
	$Se_n/SO\text{-}HPC3$ (n=60, 70)	√	/	/
	$Se_{50}/SO\text{-}HPC_3$	√	√	√
	Se and Se_{50}/AC	√	√	√
	$SO\text{-}HPC_3$	√	/	/
SIB	$Se_{50}/SO\text{-}HPC_3$	√	√	√
	Se and $SO\text{-}HPC_3$	√	/	/
PIB	$Se_{50}/SO\text{-}HPC_3$	√	√	√
	Se	√	/	/

Table S2 Specific surface areas and pore parameters of the $SO\text{-}HPC_x$ (x=0, 1, 2, 3, 4, 5)

Sample	S_{BET} (m^2 g^{-1})[a]	A_{micro} (nm)[b]	V (cm^3 g^{-1})[c]	V_{micro} (cm^3 g^{-1})[d]
$SO\text{-}HPC_0$	363.3	0.53	0.26	0.13
$SO\text{-}HPC_1$	1351.6	0.55	0.85	0.49
$SO\text{-}HPC_2$	1470.8	0.54	0.85	0.52
$SO\text{-}HPC_3$	1487.7	0.54	0.87	0.54
$SO\text{-}HPC_4$	1519.5	0.54	0.79	0.55
$SO\text{-}HPC_5$	941.8	0.56	0.40	0.34

[a]S_{BET}: the specific surface area; [b]A_{micro}: the average micropore size; [c]V: the total pore volume**;** [d]V_{micro}: the micropore volume.

Table S3 Conductivity-related data recorded by four-probe method measures

Sample	t (m)[a]	Sr (Ω/□)[b]	σ (S m^{-1})[c]
$SO\text{-}HPC_0$	/	/	/
$SO\text{-}HPC_1$	/	/	/
$SO\text{-}HPC_2$	2.7×10^{-5}	6.2×10^{4}	0.60
$SO\text{-}HPC_3$	4.3×10^{-5}	5.8×10^{3}	4.00
$SO\text{-}HPC_4$	3.5×10^{-5}	2.1×10^{4}	1.36
$SO\text{-}HPC_5$	2.7×10^{-5}	3.2×10^{4}	1.16

[a]t: thickness of material; [b]Sr: sheet resistance; [c]σ: conductivity (σ=1/(Sr×t)).

Table S4 Comparison of the electrochemical performance of Se_{50}/SO-HPC_3 (this work) with that of previously reported Se cathodes in alkali metal-Se batteries.

Sample	Loading density of Se (wt%)	Cycling performance (1C=675 mA g^{-1}) Retained capacity [mAh g^{-1}], Capacity retention rate [%]	Rate performance Average capability [mAh g^{-1}], Current density (C)	Ref
Li-Se battery				
This work	50 %	450 (RT[a]) & 77.8% (0.5 C, 1700 cycles) 219 (RT[a]) & -- (2 C, 5000 cycles) 264 (0 °C) & 53.9% (0.5 C, 400 cycles) 394 (50 °C) & 86.1% (0.5 C, 400 cycles)	225 & 20 C	
Se/C	54 %	480 (RT[a]) & 100% (0.25 C, 1000 cycles)	229 & 5 C	[1]
PPC/Se	70 %	380 (RT[a]) & 63.3% (1 C, 60 cycles)	380 & 1 C	[2]
C/Se	30 %	430 (RT[a]) & 77% (0.15 C, 250 cycles)	280 & 1.8 C	[3]
UCNS-Se	64%	347 (RT[a]) & -- (2 C, 240 cycles)	--	[4]
Se@CNx	62.5 %[a]	453 (RT[a]) & 76% (1.2 C, 400 cycles)	474 & 2.4 C	[5]
MHPCS/Se	48.68 %	261 (RT[a]) & 44.3% (0.5 C, 500 cycles)	175.4 & 5 C	[6]
NCS/Se	50 %	443 (RT[a]) & -- (0.5 C, 200 cycles)	286.6 & 5 C	[7]
Se/PCNs	70.5 %	417 (RT[a]) & 64% (1 C, 1200 cycles)	386 & 20 C	[8]
Se/CMCs	50 %	425 (RT[a]) & -- (0.2 C, 100 cycles)	218.1 & 5 C	[9]
Se@PPy	60 %	399 (RT[a]) & -- (0.2 C, 100 cycles)	238 & 2 C	[10]
Se/CNTs-M	73.3 %	428 (RT[a]) & 80% (1 C, 500 cycles)	390 & 5 C	[11]
Se/C (PAN)	56.4 %	240 (RT[a]) & -- (0.15 C, 50 cycles)	187 & 0.74 C	[12]

TP-NCF/Se	60 %	463 (RT[a]) & 87% (0.5 C, 300 cycles)	235 & 10 C	[13]
Se/CMK-3	49 %	600 (RT[a]) & 89.5% (0.1 C, 50 cycles)	310.5 & 5 C	[14]
FLSC	63.5 %	508 (RT[a]) & 64% (0.074 C, 300 cycles)	389 & 1.2 C	[15]
Se/C-700	50 %	485.3 (RT[a]) & 88.2% (0.24 C, 80 cycles)	452.3 & 1.2 C	[16]
Se@HCS200	49 %	400 (RT[a]) & 80% (0.5 C, 400 cycles)	200 & 5 C	[17]
Se–NCHPC	56.2 %	305 (RT[a]) & 70% (2 C, 60 cycles)	261 & 5 C	[18]
Se/N-CSHPC	62 %	462 (RT[a]) & 94% (0.5 C, 200 cycles)	438 & 2 C	[19]
		Na-Se battery		
This work	50 %	265 (RT[a]) & 44% (0.5 C, 600 cycles)	287 & 15 C	
Se/C	54 %	340 (RT[a]) & 70% (0.25 C, 380 cycles)	168 & 5 C	[1]
C/Se	30 %	280 (RT[a]) & 43% (0.15 C, 50 cycles)	138 & 1.8 C	[2]
Se-CCN	56.3 %	539 (RT[a]) & 88% (0.2 C, 500 cycles)	184 & 20 C	[20]
		K-Se battery		
This work	50 %	120 (RT[a]) & 22.6% (0.5 C, 200 cycles)	--	
Se/MDPC	53 %	130 (RT[a]) & 39.8% (0.2 C, 100 cycles)	101 & 1 C	[21]
c-PAN-Se	40 %	396 (RT[a]) & -- (0.2 C, 100 cycles)	116 & 10 C	[22]

[a]RT: Room Temperature (~25 °C).

References

[1] C. Luo, Y. Xu, Y. Zhu, Y. Liu, S. Zheng, Y. Liu, A. Langrock, C. Wang, *ACS Nano*, 2013, **7**, 8003-8010.

[2] Z. Zheng, Q. Su, H. Xu, Q, Zhang, H. Ye, Z. Wang, *Mater, Lett.*, 2019, **244**, 134-137.

[3] C. Luo, J. Wang, L. Suo, J. Mao, X. Fan, C. Wang, *J. Mater. Chem. A*, 2015, **3**, 555-561.

[4] W. Jin, H. Li, J. Zou, S. Inguva, Q. Zhang, S. Zeng, G. Xu, X. Zeng, *Mater, Lett.*, 2019, **252**, 211-214.

[5] Q. Cai, Y. Li, Li, Q. Li, J. Xu, B. Gao, X. Zhang, K. Huo, P. K. Chu, *Nano Energy*, 2017, **32**, 1-9.

[6] T. Liu, C. Dai, M. Jia, D. Liu, S. Bao, J. Jiang, M. Xu, C. M. Li, *ACS Appl. Mater. Inter.*, 2016, **8**, 16063-16070.

[7] Z. Li, L. Yin, Nanoscale, 2015, **7**, 9597-9606.

[8] Z. Li, L.Yuan, Z.Yi, Y. Liu, Y. Huang, *Nano Energy*, 2014, **9**, 229-236.

[9] T. Liu, M. Jia, Y. Zhang, J. Han, Y. Li, S. J. Bao, D. Liu, J. Jiang, M. Xu, *J. Power Sources*, 2017, **341**, 53-59.

[10] Z. Yi, L. Yuan, D. Sun, Z. Li, C. Wu, W. Yang, Y. Wen, B. Shan, Y. Huang, *J. Mater. Chem. A*, 2015, **3**, 3059-3065.

[11] N. Feng, K. Xiang, L. Xiao, W. Chen, Y. Zhu, H. Liao, H. Chen, *J. Alloy. Compd.*, 2019, **786**, 537-543.

[12] L. Liu, Y. Hou, Y. Yang, M. Li, X. Wang, Y. Wu, *RSC Adv.*, 2014, **4**, 9086-9091.

[13] S,-K, Parka, J,-S, Park, Y. C, Kang, *Mater. Charact.*, 2019, **151**, 590–601.

[14] C. P. Yang, S. Xin, Y. X. Yin, H. Ye, J. Zhang, Y. G. Guo, *Angew. Chem. Int. Ed.*, 2013, **52**, 8363-8367.

[15] Y. Xia, C. Lu, R. Fang, H. Huang, Y. Gan, C. Liang, J. Zhang, X. He, W. Zhang, *Electrochem. Commun.*, 2019, **99**, 16-21.

[16] C. Zhao, L. Xu, Z. Hu, S. Qiu, K. Liu, *RSC Adv.*, 2016, **6**, 47486-47490.

[17] R. Pongilat, K. Nallathamby, *J. Phys. Chem. C*, 2019, **123**, 5881-5889.

[18] Y. Qu, Z. Zhang, S. Jiang, X. Wang, Y. Lai, Y. Liu, J. Li, *J. Mater. Chem. A.*, 2014, **2**, 12255-12261.

[19] J,-P, Song. L. Wu, W,-D, Dong, C.-F. Li, L.-H. Chen, X. Dai, C. Li, H. Chen, W. Zou, W.-B. Yu, Z.-Y. Hu, J. Liu, H.-E. Wang, Y. Li, B.-L. Su, *Nanoscale*, 2019, **11**, 6970-6981.

[20] J. Ding, H. Zhou, H. Zhang, T. Stephenson, Z Li, D. Karpuzov, D. Mitlin, *Energy Environ. Sci.*, 2017, **10**, 153-165.

[21] X. Huang, Q. Xu, W. Gao, T. Yang, R. Zhan, J. Deng, B. Guo, M. Tao, H. Liu, M. Xu, *J. Colloid. Interf. Sci.*, 2019, **539**, 326-331.

[22] Y, Liua, Z, Tai, Q. Zhang, H. Wang, W. K. Pang, H. K. Liu, K. Konstantinov, Z. Guo, *Nano Energy*, 2017, **35**, 36-43.